

Article

Design of an Imaging Optical System for Large-Sized Stepped Shaft Diameter Detection

Jie Duan ^{1,2,*} , Jiyu Li ^{1,2}, Yundong Zhu ^{1,2}, Hongtao Zhang ^{1,2}, Yuting Liu ^{1,2} and Yanan Zhao ^{1,2}

¹ School of Opto-Electronic Engineering, Changchun University of Science and Technology, Changchun 130022, China; j15136031879@163.com (J.L.); custdong@cust.edu.cn (Y.Z.); 13844722515@163.com (H.Z.); a1306042648@163.com (Y.L.); zyn18730898817@126.com (Y.Z.)

² Zhongshan Institute of Changchun University of Science and Technology, Zhongshan 528400, China

* Correspondence: dj0321@126.com

Abstract: Addressing the prevalent issues of low accuracy, low efficiency, and poor image quality in online diameter measurement of large-sized stepped shafts, this study introduces a novel method based on a symmetrical dual-telecentric optical path utilizing dual CCDs, specifically designed for step shafts with diameters ranging from 600 mm to 800 mm. By developing and optimizing an imaging system grounded in the object-image dual-telecentric optical path principle and employing Zemax software for comprehensive analysis and optimization, this research achieves significant findings. The system's Airy disk radius is calculated at 3.204 μm ; the modulation transfer function (MTF) remains above 0.6 across various fields of view at a spatial cutoff frequency of 71.4 lp/mm, with smooth MTF curves; the field curvature is confined within 0.1 μm ; and the distortion is maintained below 0.1%, fulfilling high-quality imaging requirements. Additionally, a tolerance analysis is conducted to ensure the system's stability and reliability. Applied to an experimental setup for measuring the diameter of large-sized step shafts, the system demonstrates an improved measurement precision of 0.02 mm. This research offers a robust technical solution for the high-precision online measurement of large stepped shaft diameters, presenting significant practical implications for enhancing productivity and product quality.

Keywords: dual-telecentric principle; non-contact measurement; tolerance analysis



Citation: Duan, J.; Li, J.; Zhu, Y.; Zhang, H.; Liu, Y.; Zhao, Y. Design of an Imaging Optical System for Large-Sized Stepped Shaft Diameter Detection. *Appl. Sci.* **2024**, *14*, 3423. <https://doi.org/10.3390/app14083423>

Academic Editors: Zhi-Ting Ye, Pin Han, Chun-Hung Lai and Yi-Chin Fang

Received: 28 February 2024

Revised: 10 April 2024

Accepted: 12 April 2024

Published: 18 April 2024



Copyright: © 2024 by the authors. Licensee MDPI, Basel, Switzerland. This article is an open access article distributed under the terms and conditions of the Creative Commons Attribution (CC BY) license (<https://creativecommons.org/licenses/by/4.0/>).

1. Introduction

Large-sized stepped shafts are commonly used in large-scale mechanical equipment as positioning and installation components [1]. The online automatic detection of their diameter parameter has emerged as a crucial technology in measurement equipment research. The imaging optical system plays a vital role in detecting the diameter of these shafts and directly impacts the measurement accuracy. Currently, the widely used projection method for diameter measurement is effective for axis-like components due to its relatively simple technical implementation and the ease of designing collimating optical systems [2]. However, this method has limitations when it comes to larger diameter sizes, primarily due to the limited projection area and the small effective size of the linear array CCD used. Hence, there is a need to propose a diameter projection measurement method suitable for larger-sized diameters. Currently, optical imaging methods for measuring diameter using the projection method include parallel light imaging, collimated light imaging, and dual-CCD imaging. The parallel light imaging method is only suitable for measuring diameters in the range of 30 mm to 100 mm and is not applicable for measuring large-sized stepped shafts. The collimated light imaging method is suitable for measuring objects of various shapes, but for measuring the diameter of large-sized stepped shafts, it may require a longer focal length and a larger collimation angle to obtain clear imaging effects. In contrast, the dual-CCD imaging method utilizes two symmetric CCD sensors to capture the object's images and measure the diameter based on these images. It has higher accuracy

and real-time performance and allows for adjustment of the detection range by adjusting the distance between the two CCDs. For large-sized stepped shafts, the dual-CCD imaging method can better handle larger objects. However, further improvement is needed in terms of imaging quality. Therefore, this paper proposes the addition of a dual-telecentric optical system based on the dual-CCD imaging method.

At the beginning of the 21st century, researchers utilized projection methods for diameter measurements [3], which were improved and upgraded by subsequent studies. In recent years, many scholars have expanded upon the projection method to explore dual-telecentric optical imaging systems [4,5]. For instance, Ye Wenwei designed an optical system with dual fields of view, featuring two magnification factors, which were -0.275 and -0.1375 , respectively, primarily addressing the complications and accuracy issues associated with changing lenses of different magnifications [6]. However, this system requires 15 spherical lenses, making its structure overly complex compared to standard dual-telecentric systems. Cai Dali focused on the application requirements of machine vision in detecting the positional accuracy of pin needles, designing a dual-telecentric optical system with a depth of field of 0.5 mm, maximum distortion less than 0.1%, and telecentricity controlled within 0.007° , correcting various aberrations to enhance detection accuracy [7]. Yet, at a spatial frequency of 208 lp/mm, the lens contrast is low, with an MTF value just over 0.2, indicating poor imaging quality. Luo Chunhua proposed a dual-telecentric optical system with ultra-wide depth of field and low distortion, comprising seven spherical lenses with distortion less than 0.1% and telecentricity at a maximum of 0.013° . This system achieves industrial measurement requirements in terms of image quality with a good cost–performance ratio, even with fewer lenses [8]. However, its object-side field of view is only 60 mm, making it suitable only for measuring small diameters and not capable of measuring large-sized step shafts. Xianbin Fu introduced a method using laser scanners to measure diameters within the range of 200 mm–900 mm. However, the error margin between 2 mm and 6 mm renders it unsuitable for high-precision measurements [9].

To address these issues, this research employed the dual-telecentric principle to design a symmetrical dual-telecentric optical path dual-CCD system. This approach resolved the problems of low imaging quality and precision encountered when measuring large-sized stepped shafts. It lays the theoretical foundation for the imaging system of the large-sized stepped shaft diameter measurement experimental system and its applications, providing a feasible solution for measuring the diameter of large-sized stepped shafts.

This innovative system resolves problems such as low measurement accuracy and poor image quality caused by the misalignment between the scale position and the optical receiving surface. As a result, it establishes a solid theoretical foundation for developing large-sized stepped shaft diameter gauges. This technology was successfully applied to imaging systems for large-sized stepped shaft diameter gauges, laying the groundwork for further research in the field.

2. Optical Imaging System Principles for Large-Size Stepped Shaft Diameter Detection

2.1. Object-Space Telecentric Optical Path Design and Optimization

Telecentric optical paths can be classified into object-side telecentric, image-side telecentric, and dual-telecentric paths. The object-side telecentric path features a simple structure and a larger working distance range. However, compared to the dual-telecentric path, it exhibits greater distortion and aberration in the edge field of view. On the other hand, the image-side telecentric path provides high image quality with fewer secondary errors. Nevertheless, relative to the dual-telecentric path, it typically has a smaller working distance range and requires higher lens quality and manufacturing precision. Dual-telecentric optical systems combine the advantages of both object-side and image-side telecentric paths while avoiding the errors introduced by these paths during detection [10]. The schematic diagram is shown in Figure 1.

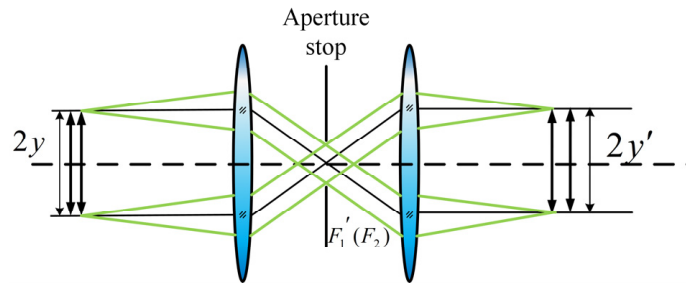


Figure 1. Schematic diagram of the double-telecentric optical path.

Dual-telecentric optical systems typically adopt a symmetric structure, with the aperture stop located at the center of the system, ensuring that the chief ray is incident and emergent parallel to the optical axis. The incident of parallel rays guarantees a sufficient depth of field in the system. The emergence of parallel rays ensures that the magnification remains constant when the working distance changes within the depth of field range, and the position of the chief ray remains unchanged. Therefore, the system has no parallax [11–14].

2.2. Symmetrical Double-Telecentric Optical Path for Large-Sized Stepped Shaft Detection

Given the measurement range of diameters from 600 mm to 800 mm, the projection method is unsuitable for measurement. Therefore, an improved method based on a dual-field-of-view optical path with dual CCDs is proposed [15], as illustrated in Figure 2. The system comprises five main components: illumination, the object under measurement, reception, signal processing, and actuation. The working principle of the system is as follows: Light emitted from the source is transformed into parallel beams through a collimation and beam expansion system. After error compensation by a plane mirror, the light is projected onto the surface of the object under measurement, forming shadows due to the object's obstruction. These shadows are captured by a dual-field-of-view optical imaging system and received by two CCD sensors. Since the size of the object under measurement exceeds the sensing area of the CCD sensors, the two CCDs can only capture the edges of the object. After edge data acquisition, the actual size of the object under measurement is determined through the signal processing module in conjunction with previously measured dimensions of standard parts. For the diameter measurement of large-sized step shafts, a wide parallel light source and a dual-field-of-view optical imaging system are required. Thus, a collimation and beam expansion system is added between the light source and the object under measurement. A plane mirror, added between the collimation and beam expansion system and the object under measurement [16], compensates for angular errors due to installation. The light source utilizes a LASER525 nm–100 nW with a laser wavelength of 525 nm. The CCD employed is a TCD1501D, with a pixel size of $7 \mu\text{m} \times 7 \mu\text{m}$.

2.3. Parameter Computation

Based on the symmetric dual-telecentric optical path detection method used in the system and considering the detection range of the large stepped shaft diameter detector (600 mm–800 mm), the maximum detection range has been increased to 820 mm in order to improve fault tolerance. The calculation of the object-side linear field of view can be expressed as follows:

$$2y = (820 - 600)/2 = 110 \text{ mm} \quad (1)$$

The TCD1501D CCD is selected, with a photosensitive receiving area of 35 mm. Additionally, the image-side linear field of view is as follows:

$$2y' = 35 \text{ mm} \quad (2)$$

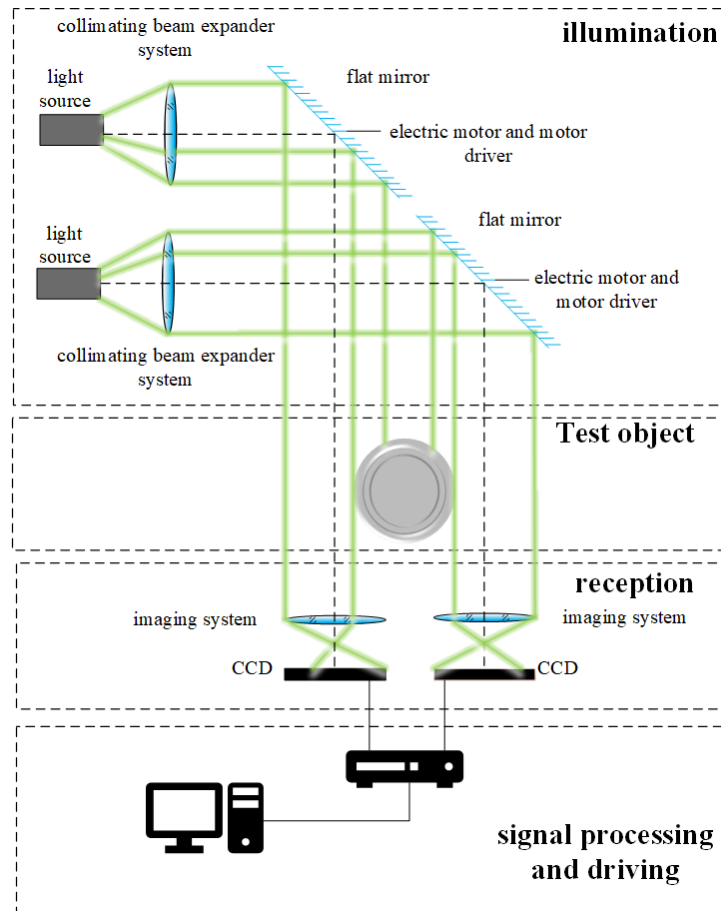


Figure 2. Schematic diagram of the diameter detection system.

Therefore, the magnification ratio [17] is the following:

$$\beta = \frac{2y'}{2y} = -0.32 \quad (3)$$

The TCD1501D CCD has a pixel size of $7 \mu\text{m} \times 7 \mu\text{m}$. Based on the Nyquist frequency [18] theory, a clear image display requires a minimum of two sampling points for each spatial frequency. Consequently, the CCD's maximum resolution is at least twice the pixel size. Therefore, the spatial frequency is defined as follows:

$$\text{spatial frequency} = \frac{1000}{2 \times \text{pixel}} \text{lp/mm} \quad (4)$$

In the equation, "pixel" represents the size of each pixel. From the above equation, it can be deduced that the maximum resolution spatial frequency of this type of CCD is 71.4 lp/mm. In order to be distinguishable by the photosensitive device, the resolution power of the designed double-telecentric system should be greater than 0.3 at 71.4 lp/mm.

The formula for calculating the Airy disk size [19] is as follows:

$$d_{\min} = 1.22\lambda_0 F \quad (5)$$

where λ_0 represents the wavelength of the laser and F is the F-number. In order to fully utilize the CCD's resolving power, it is required that the Airy disk size be smaller than the CCD pixel size. Therefore, F can be set to 10.

In a telecentric optical system, the depth of field determines the imaging clarity of the system [20] and can be represented by the object-space depth. The formula is as follows:

$$\Delta = \frac{F \times \text{pixel} \times k}{\beta^2} \quad (6)$$

where Δ represents the depth of field, β is the magnification factor, and F is the working F -number of the system. The parameter k is a specific value (commonly taken as (0.015–0.008)). Based on calculations, the depth of field for the system is determined to be 8.2 mm. Therefore, the main technical specifications of the object-image telecentric system can be found in Table 1.

Table 1. Main technical indexes of double-telecentric optical system.

System Parameters	Value
Magnification ratio	−0.32
Detection range	110 mm
Working distance	60 mm
F-number	10
Object-side telecentricity	0.1
Image-side telecentricity	0.1
Distortion	0.1%
Resolution	>30%@71.4 lp/mm

3. Design and Optimization of Double-Telecentric Optical System

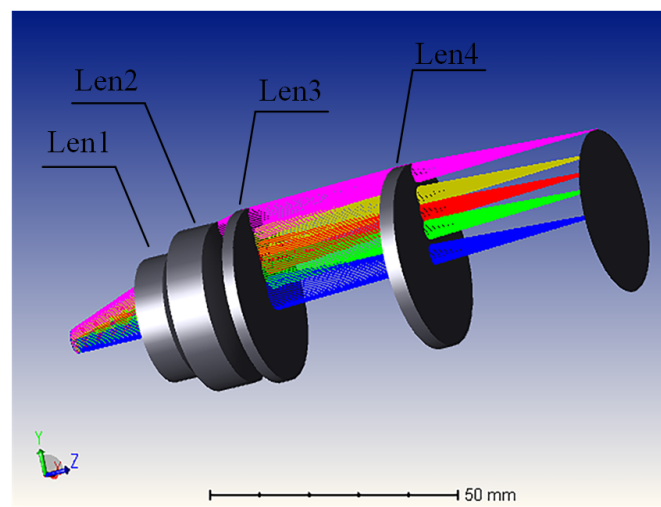
3.1. Object-Space Telecentric Optical Path Design and Optimization

In the design process of optical systems, selecting an appropriate initial structure is a critical step. Currently, there are generally two methods for determining the initial structure of a system: The first method is based on the system's relevant design specifications, utilizing the Seidel aberration theory to establish aberration balancing equations for design purposes or employing the PW method directly to design the initial structure of the system [21]. Although the method of using aberration balancing equations has notable advantages for simple system structures, it becomes computationally complex and redundant and requires a considerable workload for complex optical systems. It is difficult to achieve an efficient and high-quality system design using this method. The second method combines patent databases or existing references to determine an initial structure that meets the system's specifications for subsequent design. This approach utilizes patented structures found in optical patent databases or references as the initial structure. Regarding the complex imaging system for large-scale stepped shaft diameter detection, the second method in this article is employed to determine the initial structure of the system [22]. Firstly, a specific initial structure is chosen based on the optical design manual and the design specifications provided in Table 1. Then, scaling is performed according to the size of the image plane. Following that, an optimization function is set up to control the far focus of the object side, using the operand RANG to control the pupil distance and object distance.

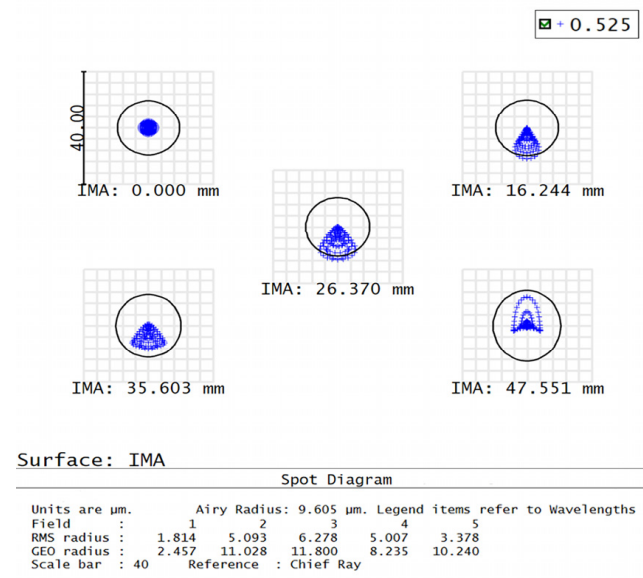
Using the operand property TTHI allows for controlling the air gap using the operand properties MNCA/MXCA/MNEA, and controlling the glass thickness is achieved using the operand properties MNCG/MXCG/MNEG. Finally, Zemax software is utilized to optimize the initial structure and generate the structure of the object-side far-focus system. The parameters are presented in Table 2, the system layout is illustrated in Figure 3a, and the spot diagram in Figure 3b.

Table 2. Structural parameters of the optimized object-space telecentric system.

	Surface	Radius	Thickness	Material	Clear Semi-Dia
0	OBJECT	Infinity	Infinity		Infinity
1	STOP	Infinity	34.609		2.402
2		−19.829	9.987	H-ZLAF71AGT	18.706
3		−27.641	0.196		25.877
4		−90.856	12.657	ZF52	34.829
5		−56.337	11.447		37.846
6		−266.608	10.569	H-ZLAF75B	46.408
7		−123.493	1.083		47.830
8		524.461	10.920	H-ZLAF52A	50.016
9		−359.472	88.534		50.252
10	IMAGE	Infinity			47.562



(a)



(b)

Figure 3. Object-space telecentric system (a) layout and (b) spot diagram.

From Figure 3b, it can be observed that this is an object-space telecentric system with an Airy disk radius of 9.605 μm . The optical system is divided into five fields of view, each

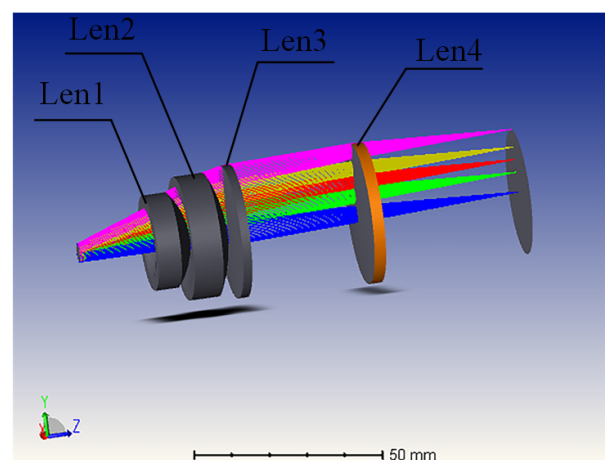
representing the image height when the rays converge at the image plane after passing through the optical system. The upper-left field corresponds to an image height of 0 mm with an RMS spot radius of 1.814 μm . The upper-right field corresponds to an image height of 16.244 mm with an RMS spot radius of 5.093 μm . The middle field corresponds to an image height of 26.370 mm with an RMS spot radius of 6.278 μm . The lower-left field corresponds to an image height of 35.603 mm with an RMS spot radius of 5.007 μm . The lower-right field corresponds to an image height of 47.551 mm with an RMS spot radius of 3.378 μm . All of these values are smaller than the Airy disk radius, indicating that the spots where the rays converge for each field of view are within the black circles shown in the diagram. These black circles represent the Airy disk radius, demonstrating that the rays converge through the system into a point rather than a diffuse spot, indicating the excellent imaging capabilities of the optical system.

3.2. Image-Space Telecentric Optical Path Design and Optimization

By scaling the object-space telecentric system based on the image plane size, using the same operands for control, and setting up an optimization function, the optical system is optimized to achieve a telecentric optical system on the image side that meets the requirements. The system parameters are shown in Table 3. The system layout diagram is shown in Figure 4a, and the spot diagram of the image-space telecentric system is shown in Figure 4b.

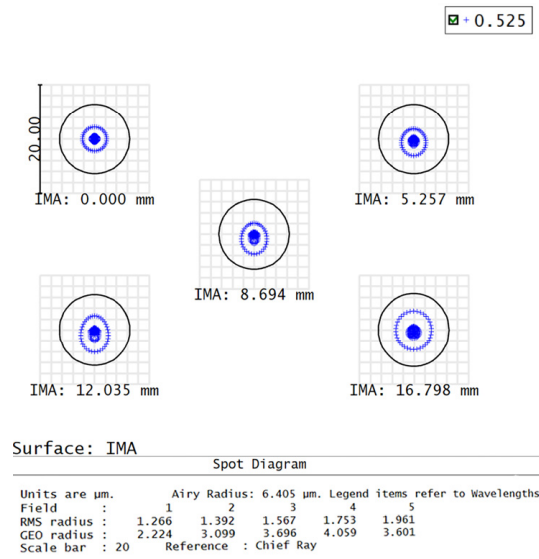
Table 3. Structural parameters of the optimized image-space telecentric system.

	Surface	Radius	Thickness	Material	Clear Semi-Dia
0	OBJECT	Infinity	Infinity		Infinity
1	STOP	Infinity	22.561		2.466
2		−14.115	7.460	H-ZLAF50D	9.276
3		−20.103	0.198		12.834
4		−44.729	9.791	H-ZLAF68B	13.840
5		−36.082	0.200		16.649
6		187.120	4.000	H-ZLAF92	17.769
7		−214.114	31.489		17.906
8		216.783	4.002	H-ZLAF76A	18.890
9		−3799.362	40.299		18.814
10	IMAGE	Infinity			16.802



(a)

Figure 4. Cont.



(b)

Figure 4. Image-space telecentric system (a) layout and (b) spot diagram.

From Figure 4b, it can be observed that this is an image-space telecentric system with an Airy disk radius of 6.405 μm. The optical system is divided into five fields of view, each representing the image height when the rays converge at the image plane after passing through the optical system. The upper-left field corresponds to an image height of 0 mm with an RMS spot radius of 1.266 μm. The upper-right field corresponds to an image height of 5.257 mm with an RMS spot radius of 1.392 μm. The middle field corresponds to an image height of 8.694 mm with an RMS spot radius of 1.567 μm. The lower-left field corresponds to an image height of 12.035 mm with an RMS spot radius of 1.753 μm. The lower-right field corresponds to an image height of 16.798 mm with an RMS spot radius of 1.961 μm. All of these values are smaller than the Airy disk radius. In the spot diagrams of each field of view, the RMS spot radius is smaller than the Airy disk radius, indicating the optical system possesses high imaging capability.

3.3. Double-Telecentric Optical Path Design and Optimization

The initial structure of a double-telecentric system is obtained. After analyzing parameters such as telecentricity, MTF, and Airy disk radius, it is determined that the system fails to meet the requirements for high-precision detection of large-sized stepped shafts. Therefore, optimization of the system is necessary.

After repeated optimization design of the system, the planning of various indicators is carried out. The system structural parameters are shown in Table 4, the system layout diagram is shown in Figure 5a, the system MTF is shown in Figure 5b, the system spot diagram is shown in Figure 5c, and the system distortion/field curve is shown in Figure 5d.

According to Figure 5b, it can be concluded that at a spatial cutoff frequency of 71.4 lp/mm, the MTF of each field of view is higher than 0.6, meeting the design requirements. According to Figure 5c, the Airy disk radius is 3.204 μm and the RMS radius is 2.660 μm. The RMS radius is smaller than the Airy disk radius, indicating that the imaging quality of the dual-telecentric system meets the requirements. The field curvature reflects the degree of bending of the image plane, and the distortion affects the accuracy of imaging [23]. According to Figure 5d, the field curvature correction is within a range of 0.1 mm, meeting the design requirements. The system distortion is less than 0.1%, also meeting the design requirements.

Table 4. Structural parameters of double-telecentric system.

	Surface	Radius	Thickness	Material	Clear Semi-Dia
0	OBJECT	Infinity	90.000		55.000
1		Infinity	0.000		57.732
2		490.438	10.000	H-ZLAF52A	57.836
3		-7741.174	0.242		57.836
4		202.545	10.000	H-ZLAF52A	56.978
5		361.121	57.115		55.927
6		96.900	19.729	H-ZF88	44.434
7		117.148	67.678		39.124
8		35.580	15.425	H-ZLAF75A	17.818
9		21.641	25.318		6.785
10	STOP	Infinity	23.171		12.750
11		-17.389	4.625	H-ZLAF50D	15.218
12		-21.193	0.769		15.218
13		-45.474	5.719	H-ZLAF68B	18.485
14		-36.297	0.206		18.485
15		-334.697	2.616	H-ZLAF92	19.836
16		-81.277	46.368		19.836
17		108.794	10.000	H-ZLAF76A	23.180
18		963.628	51.019		23.180
19	IMAGE	Infinity			17.464

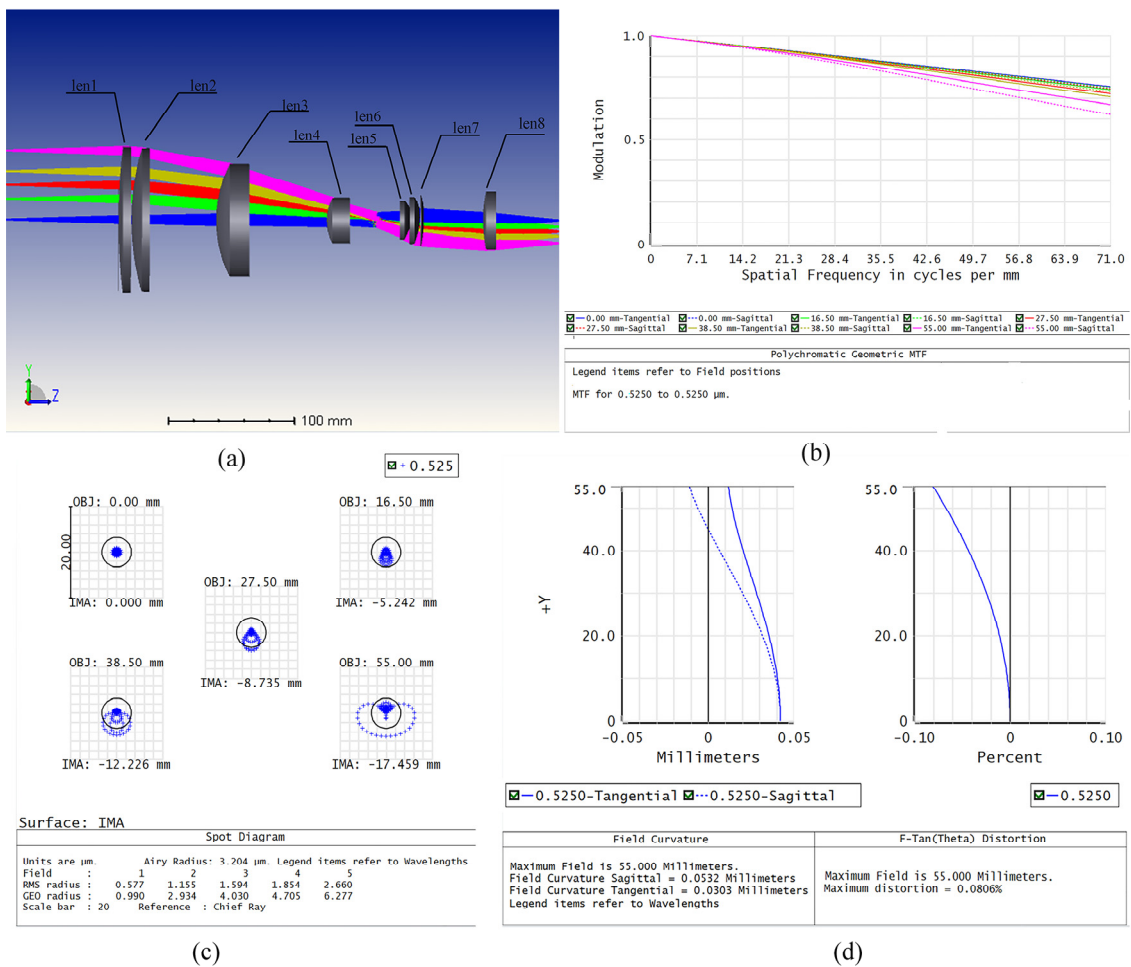


Figure 5. Dual-telecentric system. (a) Layout diagram of dual-telecentric system; (b) MTF diagram of dual-telecentric system; (c) spot diagram of dual-telecentric system; (d) field curve and distortion curve of dual-telecentric system.

4. Discussion

During the actual optical manufacturing process, there may be various errors that can affect the performance of the system. Therefore, it is necessary to use software simulations to analyze the impact of these errors on the system’s performance [24].

To ensure that the CCD sensor has a high resolution during the detection process, tolerance analyses of the imaging optical system are required to ensure that the MTF is not lower than 0.3. In this study, sensitivity analysis was used for the tolerance analyses of the imaging system, with a test wavelength of 525 nm and 500 Monte Carlo samples. The geometric mean MTF of the optical system at 71.4 lp/mm was taken as the standard. The first set of tolerance settings and analysis results are shown in Table 5, and the worst deviation types are shown in Figure 6.

Table 5. Results of the first tolerance analysis.

Aperture	±4	Tolerance Analysis	
Thickness	±0.04	Geometric Mean MTF	Result
Surface Roughness	±0.4	≥98%	0.54257240
Decenter X	±0.01	≥90%	0.58823616
Decenter Y	±0.01	≥80%	0.61704130
Tilt X	±1′	≥50%	0.66834423
Tilt Y	±1′	≥20%	0.69281911
Refractive index	±0.0003	≥10%	0.69708111
Abbe number	±0.5%	≥2%	0.70288977

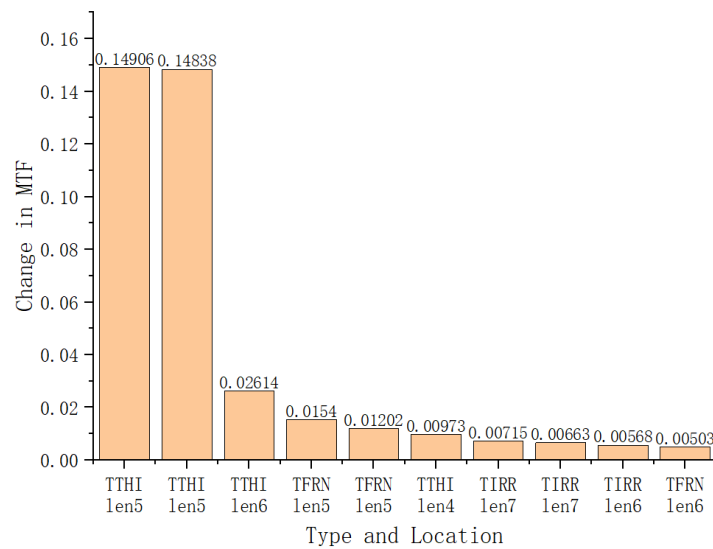


Figure 6. Worst deviation types for the first tolerance analysis.

According to the first tolerance analysis results, it can be observed that the thickness deviation of the fifth lens element (H-ZLAF50D) has the greatest impact on the MTF of the imaging system, while the influence of other parameters is relatively small. Therefore, after readjusting the tolerance settings, a subsequent analysis was conducted. The analysis results are shown in Figure 7.

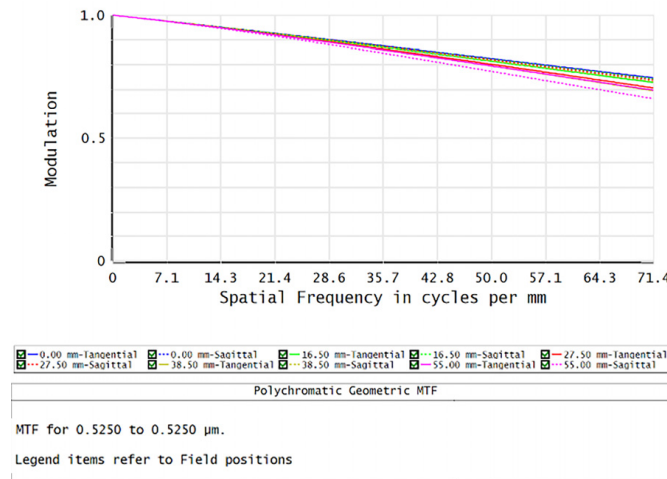


Figure 7. Results of the second tolerance analysis.

These analysis results indicate that over 98% of the samples have an MTF decrease of less than 0.1, achieving satisfactory tolerance analysis results that meet practical requirements.

5. Experiment

The dual-telecentric system designed in this study has been applied to a large-sized stepped shaft diameter measurement experimental system. This measurement system is composed of a symmetrical dual-telecentric dual-CCD system, a CCD signal processing system, and an upper-computer display system. The configuration of the large-sized stepped shaft diameter measurement system, incorporating the dual-telecentric system, is shown in Figure 8.

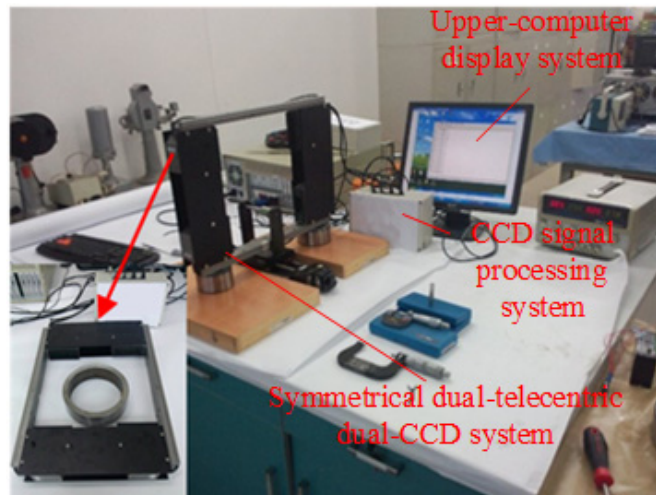


Figure 8. Experimental system for measuring the diameter of large-sized stepped shafts.

The system was tested using standard parts with diameters of 652 mm and 750 mm. The measurements were conducted using the large-sized stepped shaft diameter measurement experimental system without our imaging system installed, the same system with our imaging system installed, and a Keyence measuring instrument for comparison. The measurement results are presented in Figure 9.

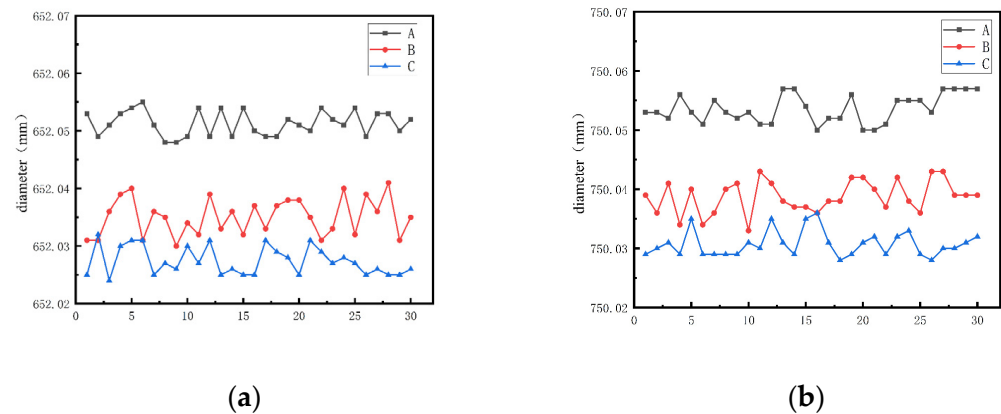


Figure 9. Measurement results. (a) Measurement of the 652 mm standard part; (b) measurement of the 750 mm standard part.

In Figure 9, 'A' represents the large-sized stepped shaft diameter measurement experimental system without the installation of our imaging system, 'B' represents the Keyence measuring instrument, and 'C' represents the large-sized stepped shaft diameter measurement experimental system with our imaging system installed. From Figure 9a, it can be observed that in the measurement of a standard component with a diameter of 652 mm, the maximum diameter measured by the large-sized stepped shaft diameter measurement experimental system without our imaging system is 652.055 mm, and the minimum diameter is 652.047 mm. The Keyence measuring instrument measures a maximum diameter of 652.041 mm and a minimum diameter of 652.30 mm. The maximum error of the large-sized stepped shaft diameter measurement experimental system with our system installed is 652.032 mm, and the minimum error is 652.024 mm. From Figure 9b, it can be observed that in the measurement of a standard component with a diameter of 750 mm, the maximum diameter measured by the large-sized stepped shaft diameter measurement experimental system without our imaging system is 750.055 mm, and the minimum diameter is 750.050 mm. The maximum diameter measured by the Keyence measuring instrument is 750.043 mm, and the minimum diameter is 750.044 mm. The maximum error of the large-sized stepped shaft diameter measurement experimental system with our system installed is 750.036 mm, and the minimum error is 750.028 mm. Through comparison, it can be seen that the installation of our imaging system significantly reduces the errors in the measurement of the stepped shaft diameter in the experimental system compared to the system without our imaging system installed. Furthermore, the errors are also reduced when compared to the Keyence measuring instrument.

6. Conclusions

A highly advanced and low-distortion dual-telecentric imaging system was designed for the purpose of large-sized stepped shaft diameter detection. The system exhibits excellent imaging quality, with a detection range of 110 mm, a working distance of 60 mm, and an Airy disk radius of 3.204 μm . At a spatial cutoff frequency of 71.4 lp/mm, the MTF transfer functions across various fields of view are all above 0.6, while the field curvature remains within 0.1 mm and distortion is controlled within 0.1%.

When applied to the experimental system for measuring the diameter of a large-sized stepped shaft using standard components, it was found that the introduction of this imaging system significantly reduced measurement errors.

Furthermore, besides its high-precision detection capabilities for large-sized stepped shafts, this system holds promising applications in fields such as projectors and laser optical paths.

Author Contributions: Conceptualization, J.D. and J.L.; methodology, J.L. and Y.Z. (Yundong Zhu); software, J.L. and H.Z.; validation, J.L., Y.L. and Y.Z. (Yanan Zhao); formal analysis, Y.Z. (Yanan Zhao); investigation, J.L.; resources, J.D.; data curation, J.L.; writing—original draft preparation, J.L.; writing—review and editing, J.D.; visualization, J.L.; supervision, Y.Z. (Yundong Zhu); project administration, J.D.; funding acquisition, J.D. All authors have read and agreed to the published version of the manuscript.

Funding: This research was funded by Zhongshan Institute of Changchun University of Science and Technology introduced innovative research team project; Project Number: CXTD2023006. And the Department of Science and Technology of Jilin Province under Grant 20210201088GX.

Institutional Review Board Statement: Not applicable.

Informed Consent Statement: Not applicable.

Data Availability Statement: The raw data supporting the conclusions of this article will be made available by the authors upon request.

Acknowledgments: The authors are grateful to the School of Optoelectronic Engineering, Changchun University of Science and Technology, and Zhongshan Institute of Changchun University of Science and Technology.

Conflicts of Interest: The authors declare no conflicts of interest.

References

1. Matar, M.S.; Alkhatib, S.E. Analysis of a stepped shaft in a rubber cracker machine. *Eng. Fail. Anal.* **2023**, *152*, 107508. [[CrossRef](#)]
2. Dvoynishnikov, S.V.; Kabardin, I.K.; Bakakin, G.V.; Rakhmanov, V.V.; Glavny, V.G. Determination of edge coordinates of cylinder in diameter measurements by the projection shadow method. In Proceedings of the 2022 IEEE 31st International Symposium on Industrial Electronics (ISIE), Anchorage, AK, USA, 1–3 June 2022; pp. 1137–1140.
3. Li, W.; Yu, Q.; Qiu, L. CCD Measuring System for Wire Diameter Using Projection Method. *Instrum. Tech. Sens.* **2001**, *1*, 34–35.
4. He, L.; Gao, Y.; Wang, G. Calibration method for CCD laser diffraction filament diameter measurement system. *J Jilin Univ. (Eng. Technol. Ed.)* **2008**, *38*, 182–184.
5. Xiao, Z.; Han, D.; An, Z. Research on non-contact diameter detection method of large shaft parts based on double CCD. *Opt. Tech.* **2015**, *41*, 463–466.
6. Ye, W.; Zhou, T.; Huang, J.; Lin, F. Design of Dual-Vision Double Telecentric Optical System Based on Machine Vision. *Laser Optoelectron. Prog.* **2020**, *1*, 57.
7. Cai, D.; Fan, J.; Wu, Q.; Chen, B.; Shen, D. Design on Bilateral Optical System with Small Depth of Field and High Resolution of machine Vision. *Laser J.* **2020**, *41*, 24–28.
8. Lou, C.; Hou, R.; Li, Y. The design of Double Telecentric Optical System in Industry. *J. Chang. Univ. Sci. Technol.* **2015**, *38*, 12–15.
9. Fu, X.; Zhang, Y.; Tao, K. The outer diameter detection and experiment of the circular forging using laser scanner. *Optik* **2017**, *128*, 281–291. [[CrossRef](#)]
10. Cao, Y. Design of Double Telecentric Lens Using Machine Vision System. *Infrared Technol.* **2022**, *44*, 140–144.
11. Zhou, T.; Huang, J.; Lin, F. Zemax-based compact dual telecentric lens design. *Symp. Nov. Optoelectron. Detect. Technol. Appl.* **2020**, *11455*, 1620–1625.
12. Li, J.; Zhang, K.; Du, J.; Li, F.; Yang, F.; Yan, W. Double-sided telecentric zoom optical system using adaptive liquid lenses. *Opt. Express* **2023**, *31*, 2508–2522. [[CrossRef](#)]
13. Mikš, A.; Novák, J. Method of initial design of a two-element double-sided telecentric optical system. *Opt. Express* **2023**, *31*, 1604–1614. [[CrossRef](#)] [[PubMed](#)]
14. Sun, W.; Xu, Z.; Li, X.; Chen, Z.; Tang, X. Three-Dimensional Shape and Deformation Measurements Based on Fringe Projection Profilometry and Fluorescent Digital Image Correlation via a 3 Charge Coupled Device Camera. *Sensors* **2023**, *23*, 6663. [[CrossRef](#)] [[PubMed](#)]
15. Li, X.; Xu, K.; Wang, S. Precision Measurement Method of Large Shaft Diameter Based on Dual Camera System. *Sensors* **2022**, *22*, 3982. [[CrossRef](#)] [[PubMed](#)]
16. Liu, Y.; Wang, C.; Song, Y.; Xie, H.; Yang, L. Optical System Design for High Precision Laser Ranging. *Appl. Opt.* **2022**, *43*, 7.
17. Wan, X.; Tao, X. Design of a Cell Phone Lens-Based Miniature Microscope with Configurable Magnification Ratio. *Appl. Sci.* **2021**, *11*, 3392. [[CrossRef](#)]
18. Luo, X.; Zhang, Z. Data recovery with sub-Nyquist sampling: Fundamental limit and a detection algorithm. *Front. Inf. Technol. Electron. Eng.* **2021**, *22*, 232–242. [[CrossRef](#)]
19. Hai-Yang, Z.; Fei, X.; Li, Z. Analysis of optical measurement precision limit for close-to-atomic scale manufacturing. *Acta Phys. Sin.* **2021**, *70*, 060703.
20. Zhu, F.; Li, Y.; Yang, Y. Infrared light field imaging technology based on Zemax simulatio. *Laser Infrared* **2023**, *53*, 945–953.

21. Gao, X.; Chen, P.; Li, M.; Ye, P.; Li, M.D. Design of Wide Field of View and Large Depth of Field Double Telecentric System. *Laser Technol.* **2017**, *41*, 182–186.
22. Liu, L.; Feng, Y.; Nong, L.; Tang, X. Design of Triple Telecentric Lens and Influence of Field of View on Optical Design. *Laser Optoelectron. Prog.* **2022**, *59*, 9.
23. Yao, L.; Liu, H. A Flexible Calibration Approach for Cameras with Double-Sided Telecentric Lenses. *Int. J. Adv. Robot. Syst.* **2016**, *13*, 82. [[CrossRef](#)]
24. Yu, Q.; Shen, Y.; Yang, Y. Design and Inspection of Wide Field of View High-Resolution Optical Inspection Mirror. *J. Zhejiang Univ. (Eng. Sci. Ed.)* **2010**, *44*, 1220–1224.

Disclaimer/Publisher’s Note: The statements, opinions and data contained in all publications are solely those of the individual author(s) and contributor(s) and not of MDPI and/or the editor(s). MDPI and/or the editor(s) disclaim responsibility for any injury to people or property resulting from any ideas, methods, instructions or products referred to in the content.